Research Article | Vol. 10, No. 10 / 1 October 2019 / Biomedical Optics Express 5198
Biomedical Optics EXPRESS

Enhanced photothermal hemostasis using dual wavelengths in an *in vivo* leporine kidney model

Sung won Kim,[1] Jieun Hwang,[2] Jason Xuan,[3] Thomas Hasenberg,[3] and Hyun Wook Kang[2,4,*]

[1]*Department of Otolaryngology-Head and Neck Surgery, Kosin University College of Medicine, Busan, South Korea*
[2]*Interdisciplinary Program of Marine-Bio, Electrical & Mechanical Engineering, Pukyong National University, Busan, South Korea*
[3]*UroPH R&D, Boston Scientific Corp., San Jose, CA 95134, USA*
[4]*Department of Biomedical Engineering and Center for Marine-Integrated Biomedical Technology (BK21 Plus), Pukyong, National University, Busan, South Korea*
[*]*wkang@pukyong.ac.kr*

Abstract: The current study investigated the hemostatic effect of dual wavelengths on *in vivo* leporine kidney tissue using 532-nm and 980-nm laser systems. Three irradiation modes, 532 nm, 980 nm, and dual (532 and 980 nm) modes, were compared to test non-contact photothermal hemostasis on 36 bleeders in the kidney models. Each bleeder was flushed with saline during the irradiation. The dual mode achieved complete hemostasis more rapidly than the single modes (4.0 ± 1.4 s for dual vs. no hemostasis for 532 nm and 10.0 ± 1.3 s for 980 nm; $p < 0.001$). Application of 60 W from the dual wavelengths expanded the surface area of the thermal lesion (up to 60%). *In vivo* dual-wavelength irradiation achieved more rapid and complete hemostasis with ~2 mm coagulation depth than the single-wavelength irradiation.

1. Introduction

Benign prostate hyperplasia (BPH) is the enlargement of stromal cells in the transition zone of the prostate, which commonly occurs in aging men. Various surgical modalities have been used to alleviate lower urinary symptoms related to BPH for resection or coagulation, including transurethral resection of the prostate (TURP), transurethral microwave thermotherapy (TUMT), and high intensity focused ultrasound (HIFU) [1]. Among the thermal modalities, 532-nm laser prostatectomy (photoselective vaporization of the prostate) has been widely accepted as a minimally invasive treatment for BPH because of selective light absorption by hemoglobin, leading to less complications than TURP [2]. Since the prostate has high vasculature, surgical urologists sometimes encounter venous or arterial bleeding during the laser prostatectomy, and the incident rate of intraoperative bleeding is up to 10% [3–5]. A number of techniques, such as increasing working distance (i.e., lowering irradiance) and rotating a fiber swiftly (i.e., reducing fluence), have been proposed to handle the bleeders effectively [6,7]. However, arterial or deep bleeding is difficult to control as the bleeder is associated with pressurized flow (pulsatile) or deeply located inside the prostate (2~3 mm below surface) [7]. Once the excessive bleeding continues and impedes vision through a cystoscope, the urologists may have to stop the procedure and convert to electrocautery to achieve complete hemostasis. In fact, the conversion to common hemostatic devices is quite cumbersome and may increase the procedure time.

The laser wavelength determines the degree of light penetration into tissue [8]. As hemoglobin strongly absorbs 532 nm light, highly vascularized prostate can experience a rapid temperature increase due to a short optical penetration of 0.8 mm [9–11]. However, the outflowing blood from a bleeder can significantly absorb and scatter the incident 532 nm light during hemostatic procedures. Thus, the remaining light cannot increase the temperature in a bleeder or reach a

#373893 https://doi.org/10.1364/BOE.10.005198
Journal © 2019 Received 26 Jul 2019; revised 3 Sep 2019; accepted 10 Sep 2019; published 16 Sep 2019

Biomedical Optics EXPRESS

deeply located bleeder, leading to incomplete hemostasis. To overcome the inherent limitations of 532 nm, our previous study combined 532 nm with a clinically available infrared wavelength of 980 nm in a perfused tissue model [12]. The infrared wavelength has a long optical penetration depth (up to 5 mm) but suffers from slow heating due to lower light absorption (e.g., 0.43 cm^{-1} at 980 nm) [13]. Presumably, the combination could compensate for the limitations of the individual wavelengths by enhancing thermal effects. Specifically, 532 nm can coagulate the outflowing blood and increase tissue surface temperature rapidly whereas 980 nm can coagulate deep tissue simultaneously. Hwang *et al*., reported that the combined wavelengths created a wide coagulation region and presented a rapid and complete hemostasis, compared to a single wavelength [12]. However, the preliminary bench study was performed in an *ex vivo* tissue model and merely proved the concept of the combined wavelengths for photothermal hemostasis. Therefore, the aim of the current study was to investigate the feasible application of dual wavelengths for the complete hemostasis in *in vivo* leporine kidney models. It was hypothesized that a combination of the two wavelengths could facilitate photothermal hemostasis due to rapid increase and wide distribution of temperature in the bleeding tissue. The hemostatic effects of three irradiation modes on the *in vivo* tissue were determined from the hemostasis time, extent of thermal coagulation, and numerical simulation.

2. Materials and methods

The current *in vivo* study used two laser systems with clinically available wavelengths for laser prostatectomy: 532 nm [quasi-continuous wave (cw) mode, GreenLight XPS, Boston Scientific, Corp., San Jose, California] and 980 nm (cw mode, custom-built). Two end-firing, 600-μm multimode, optical fibers were used to deliver each wavelength to a bleeder (defined as bleeding site) in a kidney. A hand-held device was made to integrate the two optical fibers and to firmly position them over the kidney tissue surface. Figure 1(A) shows images of the designed device (left and right top) and the overlapped irradiated spot (right bottom). The device was fabricated to deliver both the wavelengths to the same spot on the tissue surface. The two fibers were tilted at 18° and −18° for delivery of 532 and 980 nm, respectively, in order to emulate the irradiation angle of a side-firing fiber that is clinically used for laser prostatectomy. Each fiber was inserted into a channel at the end of delivery applicator (conical shape) to deflect the light coming from the fiber to the tissue. The distance between each fiber tip and the tissue surface was maintained at 3 mm as the maximum working distance used for clinical prostatectomy [7,14]. Both the fibers irradiated the equivalent beam spot in an elliptical shape (area = 1.8 mm^2) on the tissue, which was larger than the bleeder size (1.2 mm^2). A channel in the middle of the integrated device supplied saline (room temperature) at 4.4 ml/min to the bleeding lesion for convective cooling and clear visualization during the laser irradiation. It was visually confirmed that the saline rinsing alone showed no impact on hemostasis during the tests.

Figure 1(B) presents an experimental set-up for *in vivo* hemostasis testing with various irradiation modes. Six 2-month-old female New Zealand white rabbits (Hana Biotech, Suwon, South Korea) were used to simulate bleeders in kidney models. The kidney model was selected to represent glandular tissue with high vasculature that can lead to a severe bleeding condition [15–17]. All animal experiments were conducted in accordance with the guidelines of the Korean National Institutes of Health. The protocol was approved by the Institutional Animal Care and Use Committee at Pukyong National University (Permit Number: 2016-15). Before the testing, each rabbit was anesthetized by injecting 2 ml of Zoletil (Zoletil, Virbac, Carros, France) into the muscle. The rabbit underwent laparotomy with surgical instruments and was covered with a sterile cover to expose the kidney surface. A 1.5-mm diameter and 7-mm long biopsy punch (Disposable biopsy punch, Kai Medical, Seki City, Japan) was used to create a 7-mm deep bleeder in the kidney (three bleeders per kidney; total N = 36). Each bleeder was created before laser irradiation. The current study selected 20 W for 532 nm and 40 W

Biomedical Optics EXPRESS

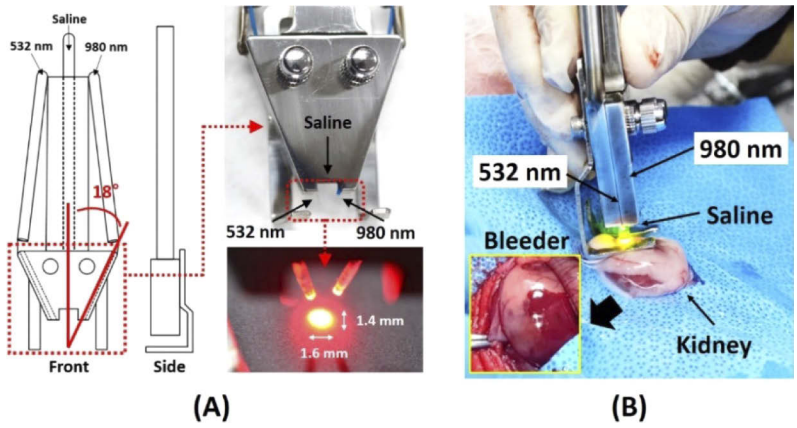

Fig. 1. *In vivo* hemostasis experiments: (A) integrated device for light delivery and (B) experimental set-up with kidney tissue

for 980 nm for the testing, based upon the previous dosimetry study in order to minimize the animal usage [12]. Three different irradiation modes were evaluated to achieve photothermal hemostasis: 20 W at 532 nm only, 40 W at 980 nm only, and simultaneous irradiation of 532 and 980 nm (i.e., dual-wavelength mode = 20-W 532 nm + 40-W 980 nm). The selected power levels solely accompanied thermal coagulation without tissue ablation. During the preliminary tests (unpublished), it was observed that higher power levels for each wavelength (i.e., higher than 20 W for 532 nm and 40 W for 980 nm) started to yield both coagulation and ablation concomitantly, aggravating bleeding. After punching, significant bleeding was visually confirmed and then, the bleeder was irradiated with each mode. The bleeders were randomly selected to minimize the effect of local perfusion changes in kidney on hemostasis. During testing, the bleeder was irradiated for 2 s, and then, the hemostatic condition of the treated bleeder was visually checked for 1 s in order to identify the inception of complete hemostasis. Coagulation time was measured and defined as the total time when the bleeding ended (complete hemostasis). Based on the preliminary animal testing, irradiation time longer than 14 s was considered "no hemostasis" as the longer irradiation aggravated the bleeding condition. Each mode was tested ten times (N = 10) for statistical analysis.

After laser treatment, the top surface of each sample was photographed using a digital camera to assess the spatial distribution of thermal coagulation. The area of the thermal lesion was defined as the area with discoloration including carbonization and coagulation around the bleeder. The area from each sample was measured using Image J (National Institute of Health, Bethesda, MD). Then, each treated tissue was fixed in a 10% neutral formalin solution for histological analysis. All the histology slides were stained with hematoxylin and eosin to evaluate the extent of the irreversible thermal coagulation at the bleeding site. Image J was used to measure coagulation depth (axial length from bottom to top of coagulated tissue) and width (lateral distance from inner wall of punctured bleeder at surface level) for each treated sample. For statistical analysis (unpaired data), the Mann Whitney U test was performed as a nonparametric method by using SPSS software (SPSS Inc., Chicago, USA), and $p < 0.05$ represents statistical significance.

Numerical simulations on distribution of temperature and thermal injury were performed to theoretically validate the thermal effects of three irradiation modes on kidney tissue by using a bioheat transfer equation as follows [12,18,19]:

$$\rho c \frac{\partial T}{\partial t} + \nabla(-k\nabla T) = \rho_b c_b \omega_b (T_b - T) + \mu_{eff} I_0 \cdot \exp(-\mu_{eff} \cdot z) \quad (1)$$

Biomedical Optics EXPRESS

where ρ (kg/m^3), c (J/kg·K), k (W/m·K) are density, specific heat, thermal conductivity of kidney tissue, respectively, T (K) the local tissue temperature, t (s) time, ρ_b (kg/m^3), c_b (J/kg·K), and k_b (W/m·K) density, specific heat, and thermal conductivity of blood, respectively, T_b (K) the temperature of arterial blood, μ_{eff} (cm^{-1}) the effective attenuation coefficient, I_0 (W/cm^2) the irradiance at the surface, and z (m) tissue depth. Effect of metabolic heat source was assumed insignificant during the simulations. The initial tissue temperature was 37 °C, and the threshold temperature of thermal coagulation in tissue was defined as 60 °C [8,20]. Both thermal and optical properties for kidney tissue were retrieved from previous studies [18,21,22]. The Arrhenius equation (i.e., first order thermal-chemical rate) was also used to describe the degree of thermal damage in tissue, by using a dimensionless parameter, Ω [8]. The parameter depends on temperature and irradiation time, which can be defined as follows:

$$\Omega = A \int_o^\tau exp[-E_a/R \cdot T]dt \tag{2}$$

where A (s^{-1}) is a pre-exponential factor, τ (s) irradiation time, E_a (J/mol) activation energy, and R (J/mol·K) universal constant. 63% of tissue undergoes irreversible thermal damage due to temperature increase when Ω becomes 1 (corresponding temperature = ~ 65 °C [6]). Quantitative differences in the coagulation dimensions (depth and width) between the simulation and experiments were evaluated to validate thermal responses from various irradiation modes. The differences were estimated by using the equation (ED-SD)/SD, where ED is the experimental dimension and SD the simulation dimension.

3. Results

Figure 2(A) demonstrates a comparison of coagulation times for three irradiation modes. 532 nm mode resulted in no hemostasis, as bleeding continued after 14 s of irradiation (280 J delivered). 980 nm mode achieved photothermal hemostasis after 10.0 ± 1.3 s (400 J delivered), but in three out of ten samples, the 980 nm treatment failed to stop bleeding. Dual mode yielded the shortest coagulation time (4.0 ± 1.4 s; 240 J delivered) with complete hemostasis ($p < 0.001$ vs. 532 nm and 980 nm). Table 1 shows a summary of hemostasis results for the three irradiation modes. Figure 2(B) compares thermal lesion areas after the three irradiation modes. Top view images of the treated leporine kidney with each mode are shown. Whitish regions represent coagulative necrosis (CN), which shows the irreversible cell death resulting from thermal coagulation. Black discoloration represents superficial carbonization (CB), where presents excessive tissue heating over 150 °C [8,13]. Coagulative necrosis occurred for all modes, whereas the 532 nm mode solely involved partial carbonization on the tissue surface, possibly resulting from localized overheating of blood. The 532-nm mode yielded the smallest thermal lesion area, while the dual mode created a 60% wider thermal lesion area than 532 nm (12.2 ± 1.2 mm^2 for 532 nm and 19.5 ± 2.1 mm^2 for dual; $p < 0.05$). No statistical difference in the thermal lesion area was found between 980 nm and the dual mode ($p = 0.09$).

Table 1. Summary of photothermal hemostasis in kidney model

Wavelength	Sample Size	Hemostasis	Time (s) [range]
		Complete / Incomplete	
Control	6	0 / 6	-
532 nm	10	0 / 10	-
980 nm	10	7 / 3	10.0 ± 1.3 [8~12]
Dual	10	10 / 0	4.0 ± 1.4 [2~6]

Figure 3(A) shows histological images of leporine kidney tissue after laser coagulation (top: 10x and bottom: 40x). Yellow dotted lines represent the region of the coagulated tissue (by

Biomedical Optics EXPRESS

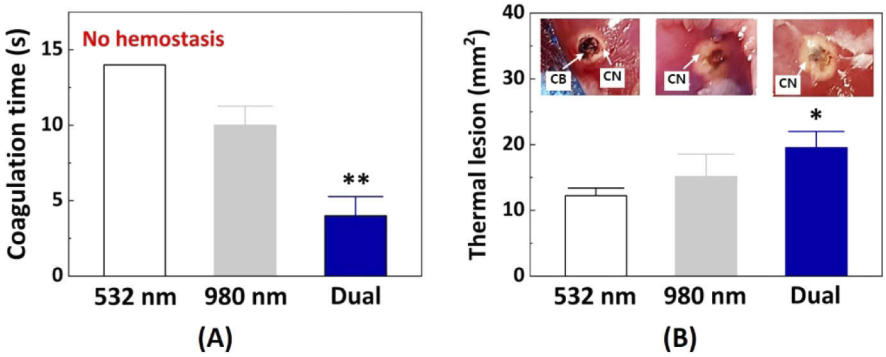

Fig. 2. Comparison of hemostatic effects for three irradiation modes: (A) coagulation time (**$p < 0.001$ vs. 532 nm and 980 nm; N = 10) and (B) thermal lesion area measured from tissue surface. Inlets represent top-view images after irradiation (*$p < 0.05$ vs. 532 nm; CB = carbonization and CN = coagulative necrosis; N = 10)

pathologist). Both 980 nm and dual modes showed deeper and wider coagulation areas than 532 nm. The bottom images at a higher magnification confirmed transformed cells and blood clots (hemorrhage) inside the tissue for the three modes. It should be noted that unlike the top-view image in Fig. 2(B), histology images from the 532 nm mode hardly showed carbonization in the tissue. Figure 3(B) presents a comparison of the coagulation dimensions (depth and width) quantified from the histology images. The dual mode created 48% deeper and 30% wider coagulation dimensions than the 532 nm (depth: $p < 0.05$ and width: $p < 0.01$). The difference in the coagulation widths between the 532 nm and the dual modes well corresponded to that in the thermal lesions [Figs. 2(B) and 3(B)]. Despite the longest irradiation time [Fig. 2(A)], 532 nm created the smallest coagulation area [Fig. 3(B)], which agrees with the smallest thermal lesion as shown in Fig. 2(A). No statistical difference in the coagulation dimensions was found between the 980 nm and dual mode (depth: $p = 0.30$ and width: $p = 0.73$).

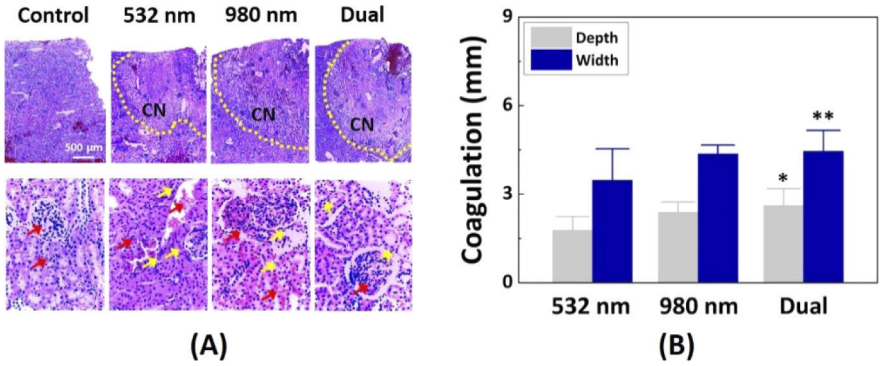

Fig. 3. Histological analysis of treated kidney tissues: (A) histology images (top: 10x and bottom: 40x) and (B) measured coagulation depth and width (*$p < 0.05$ and **$p < 0.01$ vs. 532 nm; N = 10). Note that red and yellow arrows represent hemorrhage and transformed cells, respectively.

Figure 4(A) demonstrates numerical simulation results to presents the effects of three irradiation modes on temperature (left) and thermal injury (right) distributions in the kidney. The corresponding irradiation times were 14 s for 532 nm, 10 s for 980 nm, and 4 s for dual mode, based upon the coagulation data [Fig. 2(A)]. White dotted lines represent the threshold

Biomedical Optics EXPRESS

temperature for tissue coagulation [8,13]. The 532 nm mode showed a shallow but wide temperature distribution. Conversely, the 980 nm and dual mode created a relatively deeper and wider temperature distribution. According to the simulation results, the maximum surface temperature was 100, 110, and 130 °C for the 532 nm, 980 nm, and dual mode, respectively. The white dashed lines ($\Omega = 1$ in the thermal injury images) represent a boundary where the irreversible thermal coagulation occurs [8,13]. The dual mode induced a larger area of thermal coagulation than the 532 nm mode. However, both the 980 nm and the dual modes presented comparable coagulation areas. Figure 4(B) compares spatial changes in Ω as a function of tissue depth for the three different modes, which were measured from the midline of each thermal injury image in Fig. 4(A). Evidently, the 532 nm mode yielded a shallower distribution of thermal injury whereas the dual mode expanded the thermal injury up to 2.8 mm. Figure 4(C) quantifies the coagulation differences between the simulation and the experimental results. All the irradiation modes demonstrated that the simulation predicted the thermal responses of the kidney tissue after the irradiation with less than 10% deviation, except for the coagulation depth for the 532 nm mode (around 20%).

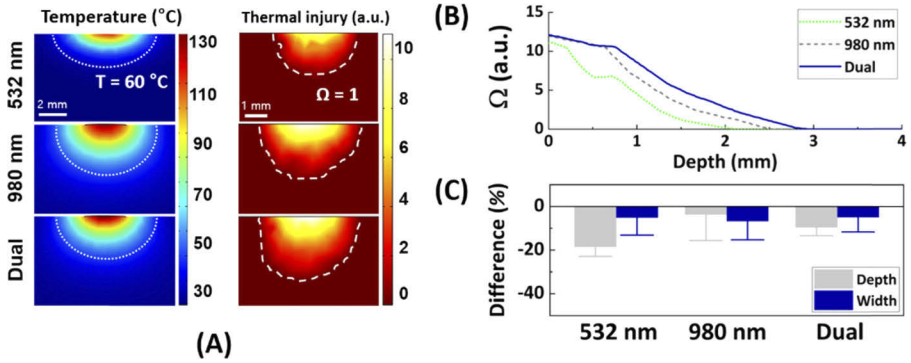

Fig. 4. Numerical simulations with three irradiation modes: (A) temperature (left) and thermal injury (right) distributions, (B) changes of thermal injury along tissue depth, and (C) comparison of thermal injury between simulation and experiment (N = 10). Note that irradiation times for 532 nm, 980 nm, and dual modes were 14, 10, and 4 s, respectively.

4. Discussion

The goal of the current research was to validate the feasible hemostasis of dual wavelengths on bleeders in *in vivo* kidney models for eventual treatment of intraoperative bleeding during laser prostatectomy. Due to rapid and wide thermal effects, the dual wavelengths facilitated complete hemostasis (Fig. 2). In fact, the coagulation time (4.0 ± 1.4 s) was comparable to or even shorter than those of electrocautery (4.5~26 s; [23–25]). The combined wavelengths were able to provide a wide thermal coagulation with a higher surface temperature and thus to reach the deeper locations of the bleeder without any physical contact (Figs. 3 and 4). The axial extent of coagulation was around 2 mm, which is similar to the coagulation thickness identified from 532-nm laser prostatectomy [10,11]. Unlike the current hemostatic devices [26], the dual irradiation can avoid any contact-induced complications, such as carbonization and tissue adhesion. Thus, application of the dual wavelengths can be a feasible method to facilitate hemostasis with a thin thermal coagulation. In addition, the complete and rapid hemostasis may secure a clear cystoscopic view during laser BPH treatment and reduce the procedure time by not having to change to hemostatic devices. However, further investigations should be performed to validate these potential clinical benefits of using the dual irradiation.

Biomedical Optics EXPRESS

The dominant mechanism for the proposed method is the enhancement of photothermal effects by irradiating two different wavelengths. As hemoglobin highly absorbs 532 nm light, 532-nm laser prostatectomy can selectively increase the temperature near the bleeding surface (above and below) to develop an optical-thermal barrier for lowering optical energy coupling and to induce small thermal lesions along with superficial hemostasis and partial carbonization [8,12]. In spite of the partial carbonization on the tissue surface, histology analysis evidenced no palpable carbonization in the cross-sectional kidney tissue [Figs. 2(B) and 3(A)]. In addition, the simulated surface temperature (100 °C) was still lower than the carbonization threshold (>150 °C) [8,13]. Thus, the outflowing blood near the bleeder could have undergone excessive local heat accumulation and could have been partially carbonized during the 532-nm irradiation. Simultaneously, 980 nm with low absorption by water can cause deep optical penetration into the tissue to expand the temperature distribution, which can eventually coagulate the peripheral tissue surrounding a bleeding channel (up to 4 mm; Fig. 3) [8,12]. However, it is conceived that the optical penetration could decrease with development of superficial tissue coagulation [11]. In spite of comparable coagulation areas in Fig. 3, the dual mode attained the complete hemostasis faster than the 980 nm mode (Table 1). Thus, the collective thermal effects on both the surface and deep tissue levels could accelerate a wide heat distribution around the expected bleeding source.

The dual wavelengths delivered a higher laser power (60 W) than the single modes (20 W for 532 nm and 40 W for 980 nm) because of the direct combination of the two wavelengths. However, the irradiation time for complete hemostasis using dual wavelengths was shorter than those of the single modes (Fig. 2), indicating a rapid and sufficient temperature rise for hemostasis without excessive thermal injury. In fact, the dual mode delivered less total energy (240 J = 60 W x 4 s) compared to the single modes (280 J = 20 W x 14 s for 532 nm and 400 J = 40 W x 10 s for 980 nm) because of the shorter hemostasis time. Numerical simulations and histological analysis confirmed that the dual mode caused a slightly higher surface temperature with no carbonization, compared to the single modes (Figs. 3 and 4). It is conceived that the surface temperature can still be lower than the carbonization threshold (>150 °C), and the irradiation could be too short to accumulate thermal energy for initiating the carbonization. Therefore, the instant temperature increase and the wide temperature distribution may be responsible for the rapid and complete hemostasis with the dual-wavelength application.

According to Fig. 4(C), the coagulation depth from 532 nm was up to 20% thinner than that from the 532 nm simulation. The difference between the simulation and experimental results could be from the partial absorption and scattering of the incident 532 nm light by blood outflowing from the tissue surface. The reduced amount of laser energy could thereby be delivered to the bleeder and merely increase temperature at the tissue surface, contributing to the limited thermal coagulation and the incomplete hemostasis. Superficial carbonization showed the accumulation of volumetric heat near the surface after a long irradiation time (up to 14 s) as there was no hemostasis. In addition, absorption coefficients varying with temperature can be responsible for the differences between the simulation and the experimental results [Fig. 4(C)]. The dynamic changes in the optical properties could reduce the amount of light absorption, leading to less development of interstitial tissue temperature and thermal coagulation in the experiments. Moreover, the effect of dynamic optical properties due to the coagulation could induce non-linear optical-thermal responses during the irradiation, possibly enhancing hemostasis with the dual wavelengths. Further numerical studies will be needed to investigate the effects of changes in the optical properties during the dual-wavelength irradiation. Both 980 nm and dual mode exhibited similar thermal behaviors in terms of degree of coagulation and temperature distribution. Unlike the dual mode, the 980 nm mode partly attained complete hemostasis (70%), possibly due to relatively slower heating [8]. Although low light absorption can cause a deep optical and thermal penetration into tissue, the tissue surface temperature increased by the 980

Biomedical Optics EXPRESS

nm mode may have been insufficient to stop the bleeding at the surface level. Thus, the dual mode can compensate for the inherent limitations of both single wavelengths for combining a rapid development of surface temperature with a deep and wide heat distribution around the bleeder as enhanced photothermal effects.

Although the current study explored the hemostatic capability of dual wavelengths *in vivo*, experimental limitations remain for laser prostatectomy. While the prostate has glandular and stromal tissues, the kidney has mainly glandular tissue. In our study, the punctured wound initiated bleeding in the kidney, but this may not fully reflect pulsatile bleeding (less pressurized). In addition, the current findings evaluated the acute responses of live tissue, such as extent of coagulation and cellular deformation. Further studies are underway to evaluate the proposed method with various bleeding models in terms of irradiation regions (i.e., 532 nm for surface and 980 nm for 2 mm below surface), blood vessel types (artery and vein), and wound shapes to confirm the efficacy of the dual-wavelength hemostasis. An additional arm of 60-W 980 nm mode will also be assessed to match the applied power of the dual mode and to compare to the current findings. Particularly, to better comprehend the underlying mechanism for the current findings, further experiments at an equivalent total power level should be performed for the dual mode. Different combinations such as 10-W 532 nm + 30-W 980 nm and 20-W 532 nm + 20-W 980 nm may elucidate whether the augmented coagulation by the dual mode results from the effect of the total power or the combination of the two wavelengths. For clinical translation, an optical beam combiner is being designed and fabricated to couple both wavelengths into a single side-firing optical fiber for simultaneous light delivery. Conceivably, the recent advancement of laser diode technology can reduce the potential cost of adding a low-power, infrared wavelength to the current 532 nm laser system. With parametric optimization, the proposed hemostatic technique will be assessed with bleeders in *in vivo* canine prostate tissue as a well-established model [9] to explore chronic healing responses of the treated tissue considering inflammatory activity, collagenous fibrosis, and delayed hemorrhage.

5. Conclusion

The current study demonstrated the potential hemostatic characteristics of irradiation with single- and dual-wavelength on bleeders in an *in vivo* kidney model for treatment of intraoperative bleeding during laser prostatectomy. Both a sudden increase of near-surface temperature and a deep thermal penetration from the dual-wavelength irradiation enhanced the collective photothermal effects, leading to the rapid and complete hemostasis with no carbonization. Future *in vivo* investigations may further substantiate these favorable features that appear to improve the hemostatic effects of the dual wavelengths on bleeders during laser prostatectomy.

Funding

Ministry of Health and Welfare, Republic of Korea (HI16C1017).

Acknowledgment

Dr. Kathy Wiemers for her editing and suggestions.

Disclosures

The authors declare that there are no conflicts of interest related to this article.

References

1. D. Mobley, A. Feibus, and N. Baum, "Benign prostatic hyperplasia and urinary symptoms: Evaluation and treatment," Postgrad. Med. **127**(3), 301–307 (2015).

Biomedical Optics EXPRESS

2. C. Welliver, S. Helo, and K. T. McVary, "Technique considerations and complication management in transurethral resection of the prostate and photoselective vaporization of the prostate," Transl. Androl. Urol. **6**(4), 695–703 (2017).
3. A. Bachmann, G. H. Muir, E. J. Collins, B. B. Choi, S. Tabatabaei, O. M. Reich, F. Gomez-Sancha, and H. H. Woo, "180-w xps greenlight laser therapy for benign prostate hyperplasia: Early safety, efficacy, and perioperative outcome after 201 procedures," Eur. Urol. **61**(3), 600–607 (2012).
4. A. Bachmann, A. Tubaro, N. Barber, F. d'Ancona, G. Muir, U. Witzsch, M. O. Grimm, J. Benejam, J. U. Stolzenburg, A. Riddick, S. Pahernik, H. Roelink, F. Ameye, C. Saussine, F. Bruyere, W. Loidl, T. Larner, N. K. Gogoi, R. Hindley, R. Muschter, A. Thorpe, N. Shrotri, S. Graham, M. Hamann, K. Miller, M. Schostak, C. Capitan, H. Knispel, and J. A. Thomas, "180-w xps greenlight laser vaporisation versus transurethral resection of the prostate for the treatment of benign prostatic obstruction: 6-month safety and efficacy results of a european multicentre randomised trial–the goliath study," Eur. Urol. **65**(5), 931–942 (2014).
5. M. Reimann, N. Fishman, I. Lichy, L. Wiemer, S. Hofbauer, Z. Almedom, J. Buckendahl, U. Steiner, T. Schlomm, F. Friedersdorff, and H. Cash, "Outcome of photoselective vaporization of the prostate with the greenlight-xps 180 watt system compared to transurethral resection of the prostate," J. Clin. Med. **8**(7), 1004 (2019).
6. G. Muir, F. Gómez Sancha, A. Bachmann, B. Choi, E. Collins, J. de la Rosette, O. Reich, S. Tabatabaei, and H. Woo, "Techniques and training with greenlight hps 120-w laser therapy of the prostate: Position paper," Eur. Urol., Suppl. **7**(4), 370–377 (2008).
7. B. Choi, S. Tabatabaei, A. Bachmann, E. Collins, J. de la Rosette, F. Gómez Sancha, G. Muir, O. Reich, and H. Woo, "Greenlight hps 120-w laser for benign prostatic hyperplasia: Comparative complications and technical recommendations," Eur. Urol., Suppl. **7**(4), 384–392 (2008).
8. A. Vogel and V. Venugopalan, "Mechanisms of pulsed laser ablation of biological tissues," Chem. Rev. **103**(2), 577–644 (2003).
9. R. S. Kuntzman, R. S. Malek, D. M. Barrett, and D. G. Bostwick, "Potassium-titanyl-phosphate laser vaporization of the prostate: A comparative functional and pathologic study in canines," Urology **48**(4), 575–583 (1996).
10. R. S. Malek, H. W. Kang, J. E. Coad, and E. Koullick, "Greenlight photoselective 120-watt 532-nm lithium triborate laser vaporization prostatectomy in living canines," Journal of endourology **23**(5), 837–845 (2009).
11. R. S. Malek, H. W. Kang, Y. S. Peng, D. Stinson, M. T. Beck, and E. Koullick, "Photoselective vaporization prostatectomy: Experience with a novel 180 w 532 nm lithium triborate laser and fiber delivery system in living dogs," J. Urol. **185**(2), 712–718 (2011).
12. J. Hwang, H. Kim, G. V. Truong, J. Xuan, T. Hasenberg, and H. W. Kang, "Dual-wavelength-assisted thermal hemostasis for treatment of benign prostate hyperplasia," J. Biophotonics **11**(4), e201700192 (2018).
13. A. J. Welch and M. J. C. van Gemert, *Optical-thermal Response of Laser-irradiated Tissue* (Plenum Press, 1995).
14. H. W. Kang, D. Jebens, R. S. Malek, G. Mitchell, and E. Koullick, "Laser vaporization of bovine prostate: A quantitative comparison of potassium-titanyl-phosphate and lithium triborate lasers," J. Urol. **180**(6), 2675–2680 (2008).
15. O. Reich, A. Bachmann, P. Schneede, D. Zaak, T. Sulser, and A. Hofstetter, "Experimental comparison of high power (80 w) potassium titanyl phosphate laser vaporization and transurethral resection of the prostate," J. Urol. **171**(6 Part 1), 2502–2504 (2004).
16. R. G. Hindley, N. J. Barber, K. Walsh, A. Petersen, J. Poulsen, and G. H. Muir, "Laparoscopic partial nephrectomy using the potassium titanyl phosphate laser in a porcine model," Urology **67**(5), 1079–1083 (2006).
17. J. K. Anderson, M. R. Baker, G. Lindberg, and J. A. Cadeddu, "Large-volume laparoscopic partial nephrectomy using the potassium-titanyl-phosphate (ktp) laser in a survival porcine model," Eur. Urol. **51**(3), 749–754 (2007).
18. M. Mesradi, A. Genoux, V. Cuplov, D. Abi Haidar, S. Jan, I. Buvat, and F. Pain, "Experimental and analytical comparative study of optical coefficient of fresh and frozen rat tissues," J. Biomed. Opt. **18**(11), 117010 (2013).
19. T. H. Nguyen, S. Park, K. K. Hlaing, and H. W. Kang, "Temperature feedback-controlled photothermal treatment with diffusing applicator: Theoretical and experimental evaluations," Biomed. Opt. Express **7**(5), 1932–1947 (2016).
20. M. A. Ansari, M. Erfanzadeh, and E. Mohajerani, "Mechanisms of laser-tissue interaction: Ii. Tissue thermal properties," J. Lasers Med Sci. **4**, 99–106 (2013).
21. J. W. Valvano, J. R. Cochran, and K. R. Diller, "Thermal conductivity and diffusivity of biomaterials measured with self-heated thermistors," Int. J. Thermophys. **6**(3), 301–311 (1985).
22. F. A. Duck, *Physical Properties of Tissue* (Academic Press, 1990).
23. A. Shabbir and D. Dargan, "Advancement and benefit of energy sealing in minimally invasive surgery," Asian J Endosc Surg **7**(2), 95–101 (2014).
24. G. W. Hruby, F. C. Marruffo, E. Durak, S. M. Collins, P. Pierorazio, P. A. Humphrey, M. M. Mansukhani, and J. Landman, "Evaluation of surgical energy devices for vessel sealing and peripheral energy spread in a porcine model," J. Urol. **178**(6), 2689–2693 (2007).
25. W. L. Newcomb, W. W. Hope, T. M. Schmelzer, J. J. Heath, H. J. Norton, A. E. Lincourt, B. T. Heniford, and D. A. Iannitti, "Comparison of blood vessel sealing among new electrosurgical and ultrasonic devices," Surg Endosc **23**(1), 90–96 (2009).
26. C. Song, B. Tang, P. A. Campbell, and A. Cuschieri, "Thermal spread and heat absorbance differences between open and laparoscopic surgeries during energized dissections by electrosurgical instruments," Surg Endosc **23**(11), 2480–2487 (2009).